

EPR probing of low temperature structural phases of Rb_2ZnCl_4 crystals with Tl^0 and Tl^{2+} centers

M. Stefan* and S. V. Nistor

National Institute for Material Physics, P.O. Box MG-7 Magurele-Bucuresti, RO-077125, Romania

E. Goovaerts and D. Schoemaker

Physics Department—Campus Drie Eiken, University of Antwerp, B-2610 Antwerpen (Wilrijk), Belgium

(Received 12 May 2003; revised manuscript received 16 October 2003; published 19 March 2004)

Thallium related paramagnetic centers of Tl^{2+} ($6s^1$) and Tl^0 ($6p^1$) type were produced by low temperature x-ray irradiation in ferroelectric $\text{Rb}_2\text{ZnCl}_4:\text{Tl}$ single crystals. Extensive EPR investigations have been performed in order to elucidate their intrinsic properties and sensitivity as paramagnetic probes for structural phase transitions studies. Compared to the s -type Tl^{2+} centers, already used in many such studies, it was found that the p -type Tl^0 centers are much more sensitive to the small variations in the local crystal field associated with these transformations. Their EPR spectra provided information about the unit cell tripling in the $P2_1cn$ phase, as well as the symmetry lowering and lattice dynamics in the $C1c1$ phase. The temperature induced, continuous changes observed in the EPR spectra of both Tl^0 and Tl^{2+} centers were explained by the influence of the soft modes responsible for the 74-K structural phase transition.

DOI: 10.1103/PhysRevB.69.104107

PACS number(s): 77.80.Bh, 61.80.Cb, 61.82.Ms, 76.30.Mi

I. INTRODUCTION

Rb_2ZnCl_4 is a particularly effective test system for studying structural phase transitions (SPTs), due to the presence of several such transitions with decreasing temperature.¹ The high temperature normal phase is paraelectric, with an orthorhombic ($Pm\bar{c}n$) structure and the number of structural units per unit cell $Z=4$. At $T_I=303$ K a first transition to an incommensurate (INC) phase takes place. At $T_C=192$ K the system passes into a commensurate orthorhombic ($P2_1cn$) ferroelectric phase, characterized by a tripling of the unit cell along the c direction with respect to the first phase and $Z=12$. Another transition to a monoclinic ($C1c1$) ferroelectric phase takes place at $T_M=74$ K, with the unit cell further doubling along both a and b directions ($Z=48$).²

Although this compound was intensively studied by various methods, the electron paramagnetic resonance (EPR) data about it are very scarce, as regards both point defects studies and SPT monitoring. The reported defect studies were concerned with the intrinsic self-trapped hole $V_k(\text{Cl}_2^-)$ centers analyzed in the commensurate phase,³ as well as with Cd^+ ($5s^1$) (Ref. 4) and Cu^{2+} ($3d^9$) (Ref. 5) impurity centers. The SPT studies in Rb_2ZnCl_4 were focused mostly on the $P2_1cn \leftrightarrow \text{INC}$ and $\text{INC} \leftrightarrow Pm\bar{c}n$ phase transitions, using Mn^{2+} ($3d^5$) ions as microscopic paramagnetic probes.^{6,7} Recently, the 74-K phase transition and the monoclinic ferroelectric phase were investigated by EPR, using Cu^{2+} ions as paramagnetic probes.⁸

Here we report the production and EPR properties of two other types of irradiation point defects in thallium doped Rb_2ZnCl_4 single crystals, namely the Tl^{2+} ($6s^1$) and Tl^0 ($6p^1$) centers. Their EPR spectra properties are investigated in both low temperature ferroelectric phases of Rb_2ZnCl_4 . The Tl^0 centers,⁹ which have not been observed in a noncubic crystal up to now, prove to be a very sensitive paramagnetic probe for studying the structural changes induced by the phase transitions. The SPT at 74 K is studied

using both types of thallium centers as paramagnetic probes, and the observed variations with temperature are attributed to the influence of the lattice modes.

II. EXPERIMENTAL DETAILS

High quality, transparent, and colorless Rb_2ZnCl_4 single crystals, doped in the melt with 0.2% mol TlCl , were obtained by the Czochralski technique in a closed apparatus under a pure argon atmosphere.¹⁰ Due to segregation effects, it is estimated that about 10% of the initial amount of thallium enters the Rb_2ZnCl_4 crystal lattice. Moreover, the thallium impurity distribution in the lattice, as revealed by EPR and optical absorption measurements, is nonuniform, its concentration increasing towards the bottom of the resulting single crystal. At such relatively low concentration levels it is expected that the Tl^+ ions are mainly distributed at isolated sites in the crystal lattice.

EPR measurements were performed with an X-band Bruker ESP-300E spectrometer, equipped with a continuous-flow cryostat (Oxford ESR910), allowing operation in the 260–2.5-K temperature range. Due to the large, uncontrollable temperature gradient present in such a cooling system, the temperature was measured at two points, above and below the sample, using two chromel-AuFe (0.07%) thermocouples. For this purpose a special sample holder was designed, with a thermocouple fixed at 1 cm above the sample's center. The reference was kept in liquid nitrogen. The other thermocouple, which was part of the variable temperature system, did measure the temperature in the helium flow path, at about 1 cm below the sample. The experimental temperature was determined as the average of the two measured temperatures.

The samples for the EPR measurements, of $2.5 \times 2.5 \times 5$ mm³ in size, were cut from cleaved plates, with their long (rotation) axis parallel to one of the $a < c < b$ crystal axes, as identified by Laue x-ray diffraction technique. The samples were x-ray irradiated (50 kV, 50 mA, W-cathode) at

liquid nitrogen temperature (LNT) and transferred into the microwave cavity without raising their temperature above 90 K. Some of the samples were submitted to thermal treatments (heating and quenching) previous to irradiation, for studies concerning the production properties of the paramagnetic centers.

III. PARAMAGNETIC THALLIUM CENTERS IN FERROELECTRIC Rb_2ZnCl_4

In order to use a paramagnetic center as a probe for studying SPT, information about the center's structure and localization is needed.¹¹ Optical absorption measurements on samples from the *as grown* thallium doped Rb_2ZnCl_4 single crystals evidenced the presence of two very intense absorption bands, at 226 nm and <195 nm. These bands were identified as the A- and C-like bands,¹² respectively, of the Tl^+ ($6s^2$) ions entered into the crystal lattice during the growth process.

Preliminary studies have shown that Tl^+ ions in Rb_2ZnCl_4 can trap both holes and electrons produced by radiolysis, resulting in Tl^{2+} ($6s^1$) (see Ref. 13) and Tl^0 ($6p^1$) (see Ref. 14) paramagnetic centers, respectively. Similar effects have been already observed and extensively studied in thallium doped alkali halides.^{9,15}

A. EPR characterization of the thallium centers

The thallium doped Rb_2ZnCl_4 single crystals produced EPR signals only after being x-ray irradiated at LNT. Figures 1(a) and 1(b) display the observed spectra along the main crystal axes, at two temperatures, 90 and 40 K, corresponding to the $P2_1cn$ and $C1c1$ phases of Rb_2ZnCl_4 , respectively. One can notice that the spectra exhibit different patterns at the two temperatures. The various groups of EPR lines were attributed to several paramagnetic centers of intrinsic or thallium related type.

The very intense group of lines around 350 mT, already observed in pure Rb_2ZnCl_4 crystals, has been attributed to self-trapped hole (V_k) centers.³ We found out that the intensity of the V_k centers spectrum in the thallium doped Rb_2ZnCl_4 crystals is about eight times larger than in undoped crystal samples of similar size. As in the case of alkali halides,¹⁶ this effect is due to the very efficient electron trapping by the Tl^+ ions, resulting in a large number of uncompensated holes in the lattice. The presence of the highly anisotropic and narrow (≈ 0.5 mT) EPR lines of the V_k centers proved to be very convenient, as we could use them to orientate the crystalline samples in the microwave cavity with high precision ($\pm 0.5^\circ$).

The pair of intense transitions at 600 and 750 mT, displaying small anisotropy, is typical¹⁵ for the hole trapped $6s^1$ - Tl^{2+} type centers. The EPR-line splitting, observed along the *a* and *b* directions in the $P2_1cn$ phase [see Fig. 1(a)], suggests the presence of at least two inequivalent centers. In the $C1c1$ phase [see Fig. 1(b)] the Tl^{2+} spectra change slightly, especially in the splitting pattern of the high field line, but, due to line superposition, the exact number of inequivalent centers cannot be determined.

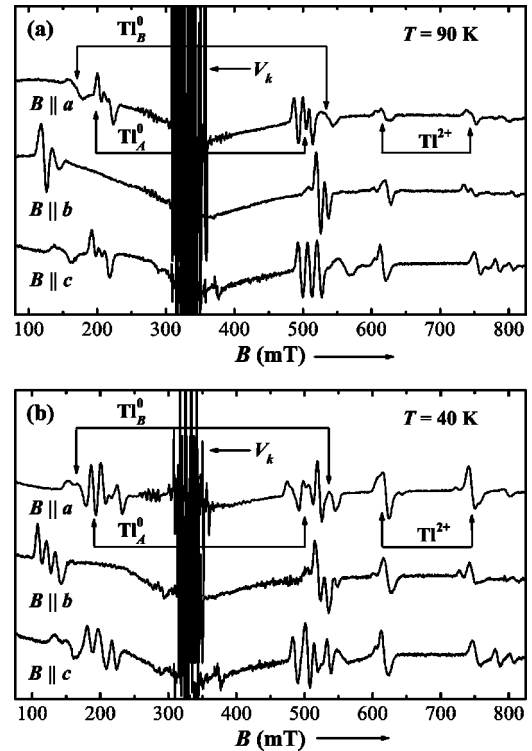


FIG. 1. EPR spectra of $\text{Rb}_2\text{ZnCl}_4:\text{Tl}$ x irradiated at LNT, measured along the main crystalline directions ($\nu = 9.44$ GHz) (a) at 90 K in the $P2_1cn$ phase and (b) at 40 K in the $C1c1$ phase.

The strongly anisotropic groups of lines at 200 and 500 mT were attributed to two types of trapped electron $6p^1$ - Tl^0 centers, called A and B, produced simultaneously with the Tl^{2+} centers. The three pairs of well-separated lines, with ≈ 6 -mT linewidth, observed along the *a* and *c* directions in the $P2_1cn$ phase, were attributed to the Tl_A^0 centers [see Fig. 1(a)]. The pair of broad lines, extending over 19 mT each, with a threefold structure discernible along the *a* axis in the $P2_1cn$ phase, were marked as Tl_B^0 . In the $C1c1$ phase the Tl^0 spectra strongly change along all three directions, in the number, positions and relative intensities of the component lines [see Fig. 1(b)].

Weak transitions belonging to other paramagnetic centers could be observed around 300 mT and in the 600–800-mT region [see Figs. 1(a) and 1(b)]. Their very low intensity did not allow a proper analysis and identification of the paramagnetic defects responsible for their presence. As shown in the case of the thallium doped alkali chlorides,^{17,18} it is expected that other thallium impurity type centers, which are not visible in the EPR spectra, could be also produced by x-ray irradiation and subsequent thermal annealing.

1. Tl^{2+} centers

Due to the relatively large linewidth (≈ 9 mT) and strong mutual overlap of the spectra, it has been possible to determine only the angular variation of the transitions belonging to the most intense Tl^{2+} center. The spin-Hamiltonian parameters were determined at 90 K in the $P2_1cn$ phase and at 40 and 26 K in the $C1c1$ phase, using the spin Hamiltonian

TABLE I. Spin-Hamiltonian parameters and direction cosines of Tl^{2+} centers relative to the cab crystal axes, in the two low temperature ferroelectric phases, at 90, 40, and 26 K. The A_i hyperfine components represent average values for the ^{203}Tl and ^{205}Tl isotopes.

Phase	$g_i(\pm 0.001)$	Direction cosine of $\hat{g}(\pm 0.04)$	$A_i(\pm 0.002)$ (T)	Direction cosines of $\hat{A}(\pm 0.04)$
$P2_1cn$ 90 K	$g_x=2.001$	0.92 -0.38 -0.01	$A_x=3.595$	0.96 -0.27 -0.11
	$g_y=2.008$	0.38 0.92 0.06	$A_y=3.599$	0.24 0.94 -0.25
	$g_z=2.000$	-0.02 -0.06 0.99	$A_z=3.601$	0.17 0.21 0.96
$C1c1$ 40 K	$g_x=2.005$	0.65 -0.68 -0.34	$A_x=3.627$	0.99 -0.07 -0.16
	$g_y=2.012$	0.51 0.72 -0.47	$A_y=3.629$	0.06 0.99 -0.10
	$g_z=2.002$	0.57 0.13 0.82	$A_z=3.630$	0.16 0.09 0.98
$C1c1$ 26 K	$g_x=2.005$	0.67 -0.43 -0.61	$A_x=3.645$	0.94 -0.34 -0.03
	$g_y=2.008$	0.40 0.90 -0.19	$A_y=3.648$	0.28 0.73 0.62
	$g_z=2.002$	0.63 -0.11 0.77	$A_z=3.647$	-0.19 -0.59 0.78

$$\frac{1}{g_0\mu_B}\mathcal{H}_S = \frac{1}{g_0}\mathbf{B}\cdot\hat{\mathbf{g}}\cdot\mathbf{S} + \mathbf{S}\cdot\hat{\mathbf{A}}\cdot\mathbf{I}. \quad (1)$$

Here all terms have the usual meaning^{15,19} and $S=I=1/2$. The spin-Hamiltonian parameters, determined by numerical fitting procedures, using the EPRNMR program,²⁰ are given in Table I. The $\hat{\mathbf{g}}$ and $\hat{\mathbf{A}}$ tensors have different orientations, as expected for a very low local symmetry. Because the isotopic effects are hidden by the large linewidth, the resulting hyperfine (hf) tensor components A_i represent the average values for the two naturally occurring ^{203}Tl and ^{205}Tl isotopes.

The values thus obtained are slightly different from the preliminary values (at 90 and 26 K) reported in Ref. 13, as the transition fields are better identified now. The angular variation in the three main planes is displayed in Figs. 2(a) and 2(b) at 90 and 40 K, respectively, in the two structural phases.

The local symmetry modification induced by the phase transition is evidenced in the different values of the parameters in the two phases. Moreover, the differences between the spin-Hamiltonian parameters at 40 and 26 K, in both principal values and orientations, show that the local crystal-line environment continues to transform in the monoclinic phase. Up to now, this effect has not been evidenced by EPR in this crystal lattice. No resolved superhyperfine structure due to the interaction of the unpaired electron with the nuclear momenta of the surrounding ions could be observed down to 2.5 K.

2. Tl^0 centers

As briefly mentioned in a preliminary report,¹⁴ three Tl^0 centers of A type were identified, with quite similar angular dependencies of the EPR transitions and mutually close spin-Hamiltonian parameters. The B -type centers seem to be also three in number, but due to the overlap of their spectra they could not be studied separately. Thus, for this type of centers only average spin-Hamiltonian values could be calculated. The subsequent analysis of the Tl^0 centers parameters suggests that the A - and B -type centers correspond to Tl^0 atoms

localized at two different lattice sites. The presence of three centers of each type is determined by the unit cell tripling in the $P2_1cn$ phase.

Based on symmetry considerations, one expects each of the Tl^0 centers from the $P2_1cn$ phase to give rise to four inequivalent centers in the $C1c1$ phase. This would amount to twelve inequivalent centers of each A - and B -type. How-

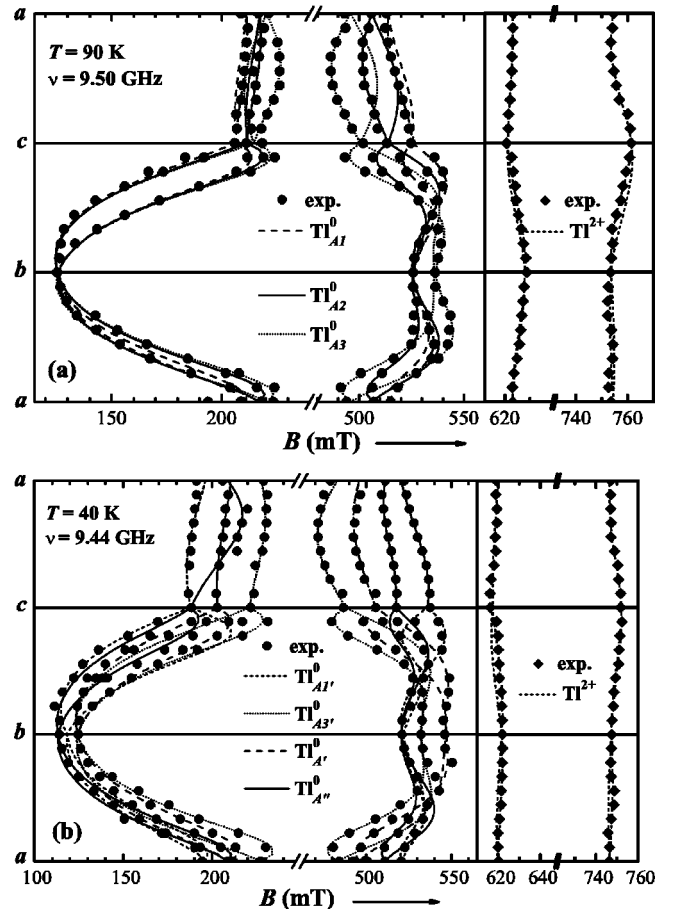


FIG. 2. Angular dependence of the Tl^0 and Tl^{2+} centers in the low temperature ferroelectric phases of $Rb_2ZnCl_4:Tl$ irradiated at LNT. (a) $P2_1cn$ phase, $T=90$ K. (b) $C1c1$ phase, $T=40$ K.

TABLE II. Spin-Hamiltonian parameters and direction cosines of Tl^0 centers relative to the cab crystal axes, in the two low temperature ferroelectric phases, at 90 K and 40 K. The A_i hyperfine components represent average values for the ^{203}Tl and ^{205}Tl isotopes.

Phase	Center	$g_i (\pm 0.005)$	Direction cosines of \hat{g} (± 0.005)	$A_i (\pm 1)$ (mT)	Direction cosines of \hat{A} (± 0.005)	A_σ (mT)	ρ (mT)
$P2_1cn$ 90 K	Tl_{A1}^0	$g_x = 1.502$	0.985 0.065 -0.160	$A_x = -196$	0.718 -0.688 -0.107	50	104
		$g_y = 1.522$	-0.069 0.998 -0.018	$A_y = -187$	0.672 0.725 -0.152		
		$g_z = 1.867$	0.158 0.029 0.987	$A_z = 338$	0.182 0.037 0.983		
	Tl_{A2}^0	$g_x = 1.512$	0.856 -0.507 0.098	$A_x = -191$	0.735 -0.675 0.064	62	103
		$g_y = 1.527$	0.495 0.860 0.127	$A_y = -169$	0.656 0.732 0.184		
		$g_z = 1.888$	-0.149 -0.060 0.987	$A_z = 345$	-0.171 -0.093 0.981		
	Tl_{A3}^0	$g_x = 1.519$	0.816 0.551 0.176	$A_x = -187$	0.721 -0.692 0.040	75	103
		$g_y = 1.529$	-0.553 0.832 -0.043	$A_y = -145$	0.676 0.715 0.181		
		$g_z = 1.883$	-0.170 -0.062 0.984	$A_z = 357$	-0.154 -0.104 0.983		
	Tl_B^0	$g_x = 1.429$	0.834 0.030 0.551	$A_x = -230$	0.473 -0.720 0.507	-1	104
		$g_y = 1.555$	-0.057 0.998 0.032	$A_y = -248$	0.572 0.689 0.445		
		$g_z = 1.839$	-0.549 -0.058 0.834	$A_z = 295$	-0.670 0.080 0.738		
$C1c1$ 40 K	Tl_{A1}^0	$g_x = 1.476$	0.963 -0.007 0.269	$A_x = -188$	0.946 -0.083 -0.313	55	103
		$g_y = 1.512$	-0.025 0.998 -0.066	$A_y = -201$	0.056 0.994 -0.095		
		$g_z = 1.881$	0.268 0.070 0.961	$A_z = 343$	0.319 0.073 0.945		
	Tl_{A3}^0	$g_x = 1.531$	0.814 0.553 0.181	$A_x = -172$	0.757 -0.653 0.032	91	100
		$g_y = 1.513$	-0.565 0.825 0.016	$A_y = -127$	0.636 0.748 0.190		
		$g_z = 1.911$	-0.140 -0.115 0.983	$A_z = 364$	-0.148 -0.124 0.981		
	$\text{Tl}_{A'}^0$	$g_x = 1.518$	0.742 -0.670 0.028	$A_x = -187$	0.821 -0.565 0.081	55	107
		$g_y = 1.541$	0.649 0.729 0.216	$A_y = -170$	0.545 0.818 0.182		
		$g_z = 1.821$	-0.165 -0.142 0.976	$A_z = 351$	-0.169 -0.105 0.980		
	$\text{Tl}_{A''}^0$	$g_x = 1.547$	0.858 -0.507 0.084	$A_x = -209$	0.859 -0.504 0.092	60	104
		$g_y = 1.472$	0.500 0.861 0.089	$A_y = -169$	0.490 0.860 0.143		
		$g_z = 1.895$	-0.117 -0.034 0.993	$A_z = 348$	-0.152 -0.078 0.985		

ever, due to the strong overlap of the EPR lines, the spectra observed at $T=40$ K along the main crystal axes do not exhibit more than seven individual lines with different intensities. We could identify and determine the EPR parameters of four Tl_A^0 centers, only. For two of these centers, called $A1'$ and $A3'$, the corresponding transitions could be followed throughout the whole temperature range in which the Tl_A^0 centers spectra are visible. Thus we found out that the $A1'$ and $A3'$ centers originate from the $A1$ and $A3$ centers in the $P2_1cn$ phase, respectively. The origin of the other two centers, called A' and A'' , could not be determined in the $P2_1cn$ phase. The transitions belonging to the B -type centers could not be properly identified in the $C1c1$ phase because of the overlap with the A -type centers spectra.

Table II shows the spin-Hamiltonian parameters of the identified Tl^0 centers in the two low temperature phases. The corresponding calculated angular variations of the A -type centers are displayed in Figs. 2(a) and 2(b). The parameters were determined by fitting a spin Hamiltonian similar to Eq. (1).

In order to gain further insight into the nature of the Tl^0 centers, use is made of expressions to second order in the perturbation theory for the \hat{A} components, expressed in an axial approximation as a function of the \hat{g} components deviations $\Delta g_i = g_i - g_0$ (Refs. 21 and 22):

$$A_{\parallel} = \left(1 - \frac{1}{2} \Delta g_{\parallel}\right) A_{\sigma} + \left(2 + \frac{3}{2} \Delta g_{\perp} + \frac{1}{2} \Delta g_{\parallel}\right) \rho,$$

$$A_{\perp} = \left(1 - \frac{1}{2} \Delta g_{\parallel}\right) A_{\sigma} - \left(1 + \frac{13}{4} \Delta g_{\perp} - \frac{9}{4} \Delta g_{\parallel}\right) \rho. \quad (2)$$

In these expressions A_{σ} is the isotropic part of the hf interaction and includes both exchange polarization (dominant and negative for the free Tl^0 atom) and a positive Fermi-contact contribution caused by s mixing, if the Tl^0 atom happens to be positioned in a crystal field with a strong odd component. The anisotropic part of the hf tensor is $\rho = (2/5)(\mu_N/I)\langle r^{-3} \rangle_{6p}$, an atomic property which is less influenced by the nature of the crystal field, being more or less constant for various Tl^0 defects.

The numerical values of ρ and A_{σ} resulting from such an analysis applied to the present data are given in Table II. The z -principal value was identified with the parallel parameter for both \hat{g} and \hat{A} , while the perpendicular parameter was taken as the average of the x - and y -principal values. As it turns out, the A - and B -type Tl^0 centers can be well distinguished by the value of the isotropic contribution A_{σ} , which for the A -type centers is positive and large, while for the B -type center it is very small. The significant difference between the respective values of A_{σ} suggests that the A - and

B-type centers occupy different sites in the host lattice. The isotropic contribution A_σ calculated for the four centers in the $C1c1$ phase falls well within the range of values corresponding to the *A*-type centers (see Table II). As expected, the anisotropic contribution ρ is almost the same for all centers and very close to the values determined for the Tl^0 -type centers in other host lattices.²² The differences in the A_σ values, especially for the Tl_{A3}^0 center, may be determined by the increased rhombicity of the centers, which was neglected in the calculation.

B. Localization and production properties of the thallium centers

In order to determine the possible aggregation of the precursor Tl^+ ions as well as the production and decay properties of the observed paramagnetic thallium centers formed after low temperature x-ray irradiation, thermal annealing experiments were performed.

Before being x-ray irradiated at LNT the samples were heated up to 723 K (about 100 K below the melting temperature) and then quenched. Such a treatment is expected to disperse the possibly agglomerated Tl^+ ions, present in the crystalline lattice. Moreover, without affecting the quality of the crystal lattice, it ensures the thermal resetting of any irradiation defects from previous experiments. The subsequent spectra did not exhibit any difference in the intensity or pattern from the spectra of the unheated samples, pointing to the absence of the aggregation phenomena. The aggregation is usually associated with the presence of neighboring charge-compensating vacancies, occurring for the substitution of a lattice ion with an impurity with different charge state.

Pulse annealing experiments have been also performed in order to determine the structure, formation and decay properties of the observed paramagnetic centers. In such experiments the x-ray irradiated sample was heated at a certain annealing temperature for 5 min, and then quenched back to 80 K, where the spectra were recorded. The range of annealing temperatures included the decay temperature of the V_k centers in Rb_2ZnCl_4 (≈ 120 K)³ and the onset of the thermal diffusion of the anion vacancies (≈ 190 K).⁴ Figure 3 displays the evolution with the annealing temperature of the relative EPR line intensities, reflecting the variation of the relative concentrations of the corresponding paramagnetic centers in the crystal.

The V_k centers concentration begins to diminish around 110 K and totally decays at about 130 K. In this temperature range the concentration of all observed centers undergoes significant changes. Part of the holes released by the V_k centers decay are trapped at Tl^+ ions, increasing thus the concentration of the Tl^{2+} centers. Another part recombines with the electrons trapped at the Tl^0 centers, resulting in a proportional decrease in the concentration of both Tl_A^0 - and Tl_B^0 -type centers. As the annealing temperature is further increased, the Tl^{2+} and Tl^0 centers concentrations exhibit a similar variation, with a steep decay above 180 K, pointing to a possible mutual recombination mechanism. No change in the

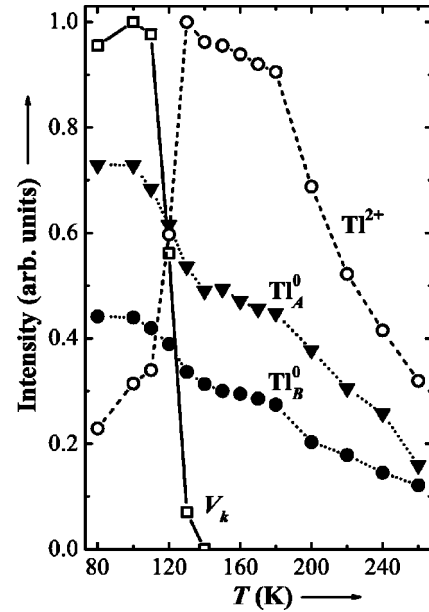


FIG. 3. Evolution with annealing temperature of the paramagnetic centers produced in $Rb_2ZnCl_4:Tl$ single crystals by x irradiation at LNT.

EPR spectra, ascribable to a vacancy movement in the vicinity of the thallium centers, could be observed in all these experiments.

With the data at hand we can discuss the structure and localization of the paramagnetic thallium centers in Rb_2ZnCl_4 . During the growth process, thallium enters the crystal lattice as monovalent Tl^+ ($6s^2$) ions. The absence of aggregation effects strongly suggests that the nonparamagnetic Tl^+ ions settle in positions where they do not need charge compensation, or the compensation takes place at a distance. At these positions they trap holes and electrons released by x-ray irradiation and transform into the paramagnetic Tl^{2+} and Tl^0 centers, respectively.

In discussing the possible localization of the Tl^+ ions in the crystal lattice one should keep in mind that in the high temperature $Pm\bar{c}n$ phase of the Rb_2ZnCl_4 crystals there are three cationic positions, namely, Zn^{2+} , $Rb^+(1)$ and $Rb^+(2)$, which can accommodate these ions. The $Rb(2)$ site is characterized by a closer packing, with shorter distances to the surrounding Cl^- ions²³ than $Rb^+(1)$. As shown in Sec. III A, two major, different types of both Tl^{2+} and Tl^0 centers were observed. This situation can arise from the localization of the precursor Tl^+ ions either at the two Rb^+ sites, or at the Zn^{2+} and Rb^+ sites. Unfortunately, in the absence of a resolved superhyperfine structure the occupied sites cannot be clearly identified. One can only speculate that the low symmetry Rb^+ sites seem to be more suitable hosts for the Tl^+ ions, due to both electrical charge and ionic radius match [$r(Rb^+) = r(Tl^+) = 1.47$ Å, while $r(Zn^{2+}) = 0.74$ Å]. In such a case, the two different Tl^{2+} centers would be localized at the two inequivalent Rb^+ sites. For the Tl^0 centers, the differences between the *A* and *B* types can be well explained by the localization of the Tl_A^0 centers at $Rb(2)$ sites and of the Tl_B^0 centers at $Rb(1)$ sites. Indeed, the looser sur-

rounding of Rb(1) induces weaker interactions with the ligand field and thus a lower differentiation between the three Tl_B^0 centers, while the stronger interactions at Rb(2) sites would account for the neat differentiation between the three Tl_A^0 centers in the $P2_1cn$ phase.

IV. THALLIUM CENTERS AS PARAMAGNETIC PROBES FOR SPT

The EPR spectra of both Tl^{2+} and Tl^0 centers can be observed in a temperature range extending over the two ferroelectric phases of Rb_2ZnCl_4 , i.e., up to 250 and 210 K, respectively. At higher temperatures, the EPR lines become indistinguishable, as a result of both thermally induced decay and line broadening effects.

The ns^1 -type Tl^{2+} centers have often been employed for SPT studies on different crystals, including some belonging to the Rb_2ZnCl_4 crystalline family.¹⁵ The temperature range in which they are stable suggests their possible use to probe the less investigated phase transition at 74 K and the low temperature $C1c1$ phase. On the other hand, the higher sensitivity of the Tl^0 centers to small variations in the crystalline environment makes them eminently suited as paramagnetic probes for such a study.

The presence of both Tl^{2+} and Tl^0 centers in the same crystal is also a most convenient occasion for comparing the sensitivity in SPT investigations of the np^1 Tl^0 paramagnetic probes with that of the better known ns^1 -type probes.

A. Temperature variation of the Tl^{2+} and Tl^0 EPR spectra

Careful EPR measurements vs temperature were performed, with the magnetic field parallel to the a and b axes, respectively, along which the unit cell is doubled in the $C1c1$ phase. The spectra were recorded with a 2° temperature step, which was decreased to 1° in a ± 10 K range around both $T_M=74$ K and $T_C=192$ K transition temperatures.

Figure 4 displays the EPR spectra measured along the a crystal axis at various temperatures, in a magnetic field range which includes the EPR transitions from both Tl^{2+} and Tl^0 centers. The 7–195-K temperature range includes both $C1c1$ and $P2_1cn$ phases and the transition point into the incommensurate phase. The temperatures selected in the figure correspond to significant changes in the spectra. Special attention was paid to the $P2_1cn \leftrightarrow C1c1$ transition region, from 71 to 74 K, where the spectra are displayed in steps of 1 K.

The Tl^0 spectra exhibit in the whole temperature range a strong variation in the number, positions and intensities of the EPR component lines (see Fig. 4). These changes are more visible for the A-type centers. The maximum splitting of the Tl_A^0 spectra, which are better resolved, is reached below 20 K. The observed component lines exhibit different intensities, which can be explained as resulting from the superposition of lines originating from a larger number of centers. By raising the temperature, towards the $P2_1cn$ phase, the lines tend to collapse into a three equally intense components structure. Above 120 K the threefold structure of the spectra becomes less and less visible, until a single weak,

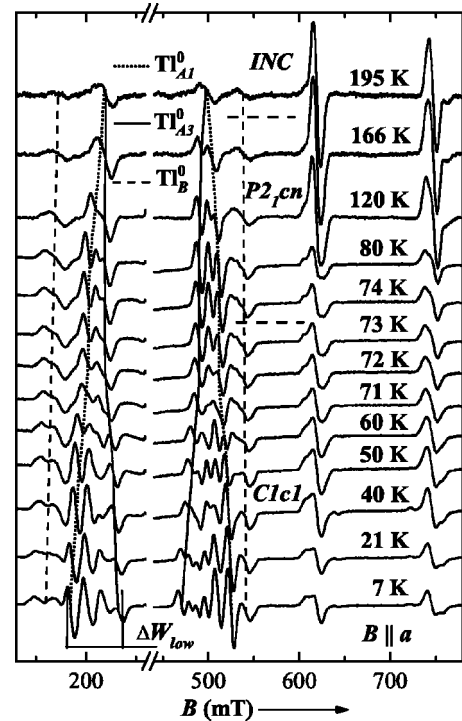


FIG. 4. EPR spectra of $Rb_2ZnCl_4:Tl$ along the a crystal axis at different measuring temperatures.

symmetrical line remains around 192 K, at the transition into the INC phase. Similar changes seem to occur in the case of the B-type centers, although in this case the separation of various component lines is not so obvious.

The observed changes in the EPR spectra of the Tl^0 centers can be attributed to the structural changes associated with the low temperature phase transitions. Indeed, the threefold structure of the spectra from both Tl_A^0 and Tl_B^0 centers can be associated with the tripling of the unit cell which takes place at 192 K, at the transition from the INC phase into the $P2_1cn$ phase. A further splitting of each line is expected to occur in the $C1c1$ phase, associated with the quadruplication of the unit cell, which leads to 12 inequivalent Tl^0 centers of each A and B type.

In order to analyze the observed collapse of the component lines into a single line, when raising the temperature from the lowest measured temperature to the transition temperature into the INC phase, we have measured the spread of the group of low field transitions belonging to the Tl_A^0 centers. As shown in the lower part of Fig. 4, the measured spread ΔW_{low} has been determined as the distance between the positions of the farthest peaks of the derivative signals. This means that the measured ΔW_{low} value represents the sum of the maximum separation between the low field lines belonging to inequivalent centers, plus the individual linewidth.

Figure 5 presents the temperature variation of ΔW_{low} . A steep decrease of ΔW_{low} with increasing temperature can be noticed in the $C1c1$ phase and also a smooth, almost linear decrease in the $P2_1cn$ phase. Around 74 K, at the $C1c1 \leftrightarrow P2_1cn$ transition, the ΔW_{low} variation becomes

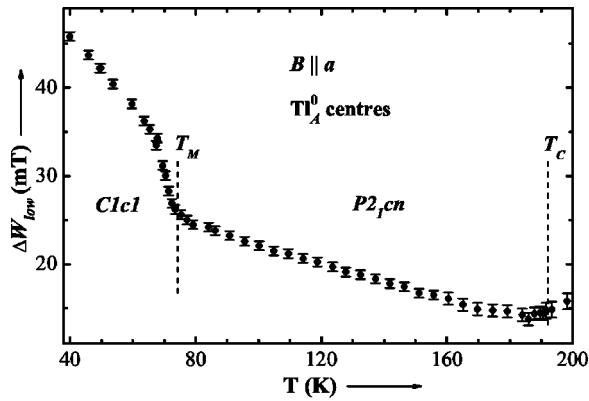


FIG. 5. Temperature dependence of the spread of the TI_A^0 -centers low field transitions group, ΔW_{low} , along the a direction, which includes the individual linewidth. The transition temperatures are marked with vertical dotted lines.

much steeper. Another change from negative to positive slope of ΔW_{low} is visible around 185 K, close to the $P2_1cn \leftrightarrow \text{INC}$ transition.

To separate the temperature induced variation of the individual linewidth from the effective lines spread, we have measured the individual linewidth for the magnetic field orientation at 7° from the c crystal axis in the (bc) plane. For this particular orientation, one component of the low field group of lines of the TI_A^0 centers is well separated from the other lines of the non-equivalent A-type centers, from the lowest attainable temperature up to 150 K. We found out that the corresponding individual linewidth exhibits an almost constant value of about 6.8 mT, up to 150 K, where the line overlaps other two triplet lines. In smaller temperature ranges we observed similar linewidth values for other, quite well separated component lines, as well. At higher temperatures, for many orientations of the sample in the magnetic field, the lines belonging to both TI^0 centers exhibit a homogeneous broadening accompanied by loss of signal amplitude, which is very likely due to thermally induced relaxational broadening effects.

Based on these results, one concludes that the continuous decrease of ΔW_{low} with temperature increase in both low temperature ferroelectric phases, up to 150 K, is due to the structural changes in the crystal lattice. At higher temperatures, close to the $P2_1cn \leftrightarrow \text{INC}$ transition, the contribution of the thermally induced line broadening effects seems to be responsible for the observed change in the slope of the ΔW_{low} vs temperature curve in Fig. 5.

One can notice from Fig. 4 that the EPR lines of the two TI^{2+} centers also exhibit a collapsing tendency as the incommensurate phase is approached. Above 160 K a single, symmetric line can be seen. The variation with temperature of the TI^{2+} spectra is, however, less dramatic than in the case of the TI^0 and the structural change at the phase transition is reflected mainly in the shifting of the line positions.

A similar behavior of the TI^{2+} spectra vs temperature was observed along the b crystal axis (see Fig. 6). The TI^0 spectra also show a collapsing tendency with increasing temperature, but, due to the strong overlap of the EPR lines from the A-

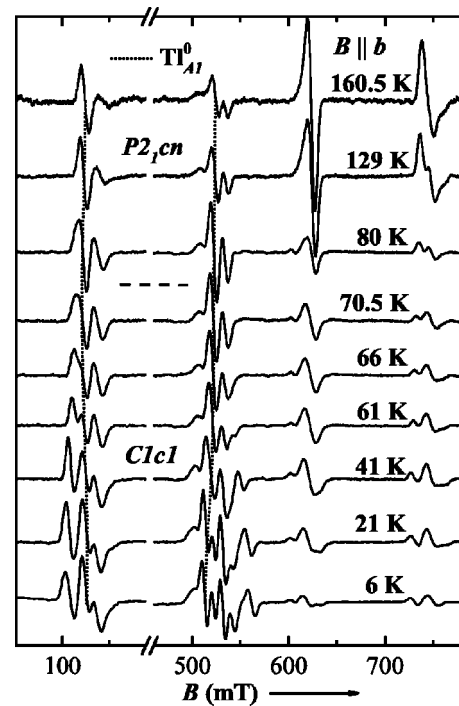


FIG. 6. EPR spectra of $\text{Rb}_2\text{ZnCl}_4:\text{Tl}$ along the b crystal axis recorded at different temperatures.

and B-type centers, both in the low field and high field regions, the analysis is more difficult.

No clear effects associated to the structural modulation characteristic to the INC phase could be observed in the EPR spectra of both TI^0 and TI^{2+} centers. In the case of the TI^0 centers, such effects are very likely masked by the thermally induced line broadening of the very weak signals, still visible for about 20 degrees above the transition point. In the case of the TI^{2+} centers, for which the thermally induced line broadening is not effective yet and the EPR lines are visible up to about 250 K, the effects associated with the structural modulation are very likely hidden into the broad, isotropic lines.

B. Lattice modes influence on the thallium centers spectra

Raman²⁴ and neutron scattering²⁵ experiments have revealed the presence of two soft modes, belonging to different representations, associated with the second order $P2_1cn \leftrightarrow C1c1$ phase transition in Rb_2ZnCl_4 . The two soft modes, called ω_{a1} and ω_b , arise from a doubly degenerate mode in the $P2_1cn$ phase, which softens at $(a^* + b^*)/2$, where a^* and b^* are the reciprocal lattice vectors. They exhibit a continuous frequency variation vs temperature in the $C1c1$ phase, similar to the temperature variation of the TI^{2+} and TI^0 centers hyperfine splitting. Consequently, we assume that both TI^{2+} and TI^0 centers are strongly coupled to the vibration modes of the lattice, in particular to the soft modes.

Analytical expressions have been previously derived to describe the influence of a ω_q soft mode on the temperature variation of the zero-field-splitting (ZFS) parameter D in the case of the $3d^5$ -type Fe^{3+} centers in KDP (see Ref. 26) and

of the hyperfine parameter for the ns^1 -type Cd^+ and Hg^+ centers in $(\text{NH}_4)_2\text{SO}_4$ (see Ref. 27). According to Tsuchida and Abe,²⁶ this influence is induced by the instantaneous displacement of the impurity ion, $u(t)$, relative to the surrounding lattice. A spin-Hamiltonian parameter P (the D parameter in their case and the hf parameter in Ref. 27), sensitive to the local field modifications, can be written as

$$P(t) = P_0 + \Delta P(u(t)), \quad (3)$$

where P_0 is a term related to the static distribution of the surrounding ions and $\Delta P(u(t))$ accounts for the variations induced by the ion displacement from the equilibrium position. By expanding $\Delta P(u(t))$ in terms of small $u(t)$, written in terms of usual phonon operators and considering the high temperature approximation, the time average of $P(t)$ becomes

$$\langle P(t) \rangle = P_0 + \kappa T \sum_q \frac{1}{\omega_q^2}, \quad (4)$$

where κ is a constant expressible in the phonon properties. Here ω_q^2 is expressed as²⁸

$$\omega_q^2(T) = \alpha(T_c - T)^\gamma + \beta^2 q^2, \quad (5)$$

where α and β are material constants, q is the soft mode wave vector, and γ is the critical exponent. Inserting Eq. (5) into Eq. (4) and integrating over the Brillouin zone, the value of $\langle P(t) \rangle$ goes as

$$\langle P(t) \rangle(T) = P_0 + P_1 T \left(1 - \frac{|T - T_c|^{\gamma/2}}{C} \arctan \frac{C}{|T - T_c|^{\gamma/2}} \right), \quad (6)$$

where $C = (\beta/\sqrt{\alpha})Q$ and Q is the Brillouin zone cut-off.

In our case the high temperature approximation $k_B T > \hbar \omega_q$ is valid for temperatures above 20 K, as the frequencies of the displacive ω_{a1} and ω_b soft modes are ≈ 11 and $\approx 12 \text{ cm}^{-1}$, respectively.²⁴

In the $P2_1cn$ phase other i modes are excited, which could influence the P parameter values. Their contribution to the temperature variation of P is expressed as $\sum_i \coth(\hbar \omega_i / k_B T)$ (see Ref. 29), which at high enough temperatures approaches a linear dependence. Thus, for $\hbar \omega_i \ll k_B T$, $P(T)$ will have a variation of the form

$$P(T) = P'_0(1 - C'T). \quad (7)$$

The thermal expansion of the lattice is also expected to contribute to the temperature dependence of the EPR parameters, especially at higher temperatures, in the $P2_1cn$ phase. As will be further shown, a linear experimental temperature dependence of the hf splitting for both types of centers in this temperature range was observed. This result suggests that either the thermal expansion contribution is negligible or both implicit and explicit contributions are linear in temperature in the first approximation.

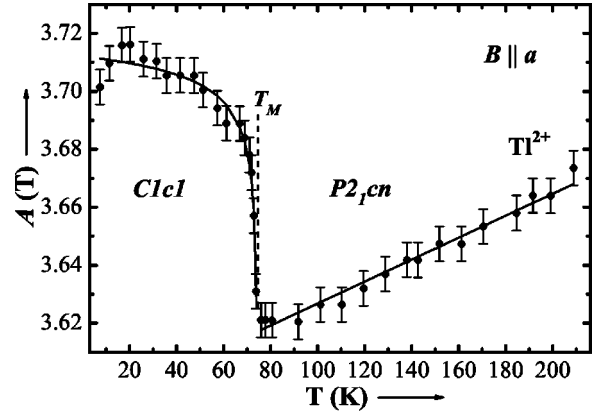


FIG. 7. Temperature dependence of the hyperfine parameter A of Tl^{2+} centers (solid circles) along the a direction in ferroelectric $\text{Rb}_2\text{ZnCl}_4:\text{Tl}$. Solid lines—the result of the fitting.

1. Tl^{2+} centers

In the case of the Tl^{2+} centers, the most temperature sensitive parameter is the very large hf splitting. Considering the small anisotropy of the hf tensor (less than 0.5%; see Table I), we calculated the hf parameter with a simple formula derived¹⁵ from the Breit-Rabi equations, approximating the centers as fully isotropic:

$$A = \frac{h\nu}{2\mu_B g_0(B_2 - B_1)} \left\{ (B_2 + B_1) \pm [(B_2 + B_1)^2 + 8(B_2 - B_1)^2]^{1/2} \right\}. \quad (8)$$

Figure 7 displays the temperature dependence of the hf parameters as calculated with this equation from the resonance fields measured along the a crystal axis. In the temperature region corresponding to the $C1c1$ phase one can notice a steep decrease of the hf parameter as the transition temperature is approached, which is attributed to the influence of the lattice modes that soften at T_M . In the $P2_1cn$ phase, an approximately linear increase of the hf parameter can be observed. No particular variation is marking the transition into the incommensurate phase at 192 K.

The analysis of the hf temperature dependence in the $C1c1$ phase has been performed considering the coupling with a soft mode only. We used expression (6) for fitting the experimental data, where the general parameter P was replaced by A . The critical temperature T_c from expression (6) was, in our case, equal to the $C1c1 \leftrightarrow P2_1cn$ transition temperature, $T_c = T_M = 74 \text{ K}$, and the γ exponent was set to the mean-field value $\gamma = 1$, as in Ref. 26. The experimental errors of about $\pm 0.5 \text{ mT}$ in the determination of the transition fields close to the phase transition and the $\pm 1 \text{ K}$ accuracy in the temperature measurements did not allow an accurate determination of γ in the critical region. The resulting parameters are given in Table III, and the calculated temperature dependence is represented in Fig. 7 with solid lines, for $T < T_M$. The deviations observed below 30 K are probably due to the fact that the high-temperature approximation is not valid anymore.

TABLE III. Fitting parameters for the soft mode induced temperature dependence along the a direction of the hf parameter in the case of Ti^{2+} center and of $\Delta B_{res} = B_2 - B_1$ in the case of Ti_{A1}^0 centers, considering $T_c = T_M = 74$ K and $\gamma = 1$.

Phase	Fitting parameters	Ti^{2+}	Ti_{A1}^0	Ti_{A3}^0
$C1c1$	P_0 (mT)	$(3.711 \pm 0.005) \times 10^3$	342.4 ± 0.5	240.0 ± 0.5
	P_1 (mT K $^{-1}$)	-1.1 ± 0.5	-0.51 ± 0.05	0.47 ± 0.05
	C (K $^{1/2}$)	4.0 ± 2.0	14.0 ± 1.0	15.0 ± 1.0
$P2_1cn$	P'_0 (mT)	$(3.589 \pm 0.005) \times 10^3$	326.2 ± 0.5	270.2 ± 0.5
	C' (K $^{-1}$)	$(-1.10 \pm 0.05) \times 10^{-4}$	$(0.70 \pm 0.01) \times 10^{-3}$	$(-0.6 \pm 0.1) \times 10^{-4}$

The temperature dependence of the Ti^{2+} hf parameter in the $P2_1cn$ phase could be well fitted with Eq. (7). The fitting parameters P'_0 and C' are given in Table III. The negative sign of the C' constant suggests that the temperature variation of the hf parameter in this phase is determined mostly by the thermal expansion of the lattice, and not by the influence of the lattice modes. It is possible that the increase in the interionic distances with temperature yields a reduction in the strength of the odd local crystalline field components responsible for admixture of the excited $6p$ state into the ground $6s$, thus inducing the observed increase of the hf parameter. However, in order to ascertain the presence of such an effect, information about the pressure dependence of the Ti^{2+} centers hf parameter would be needed.

2. Ti^0 centers

Due to the large number of inequivalent centers and the strong overlap of the corresponding EPR lines in the $C1c1$ phase, only two centers, namely Ti_{A1}^0 and Ti_{A3}^0 , could be followed throughout the whole investigated temperature range, along the a crystal axis (see Fig. 4) and just one, namely, Ti_{A1}^0 , along the b crystal axis (see Fig. 6). The pairs of transitions belonging to the Ti_{A1}^0 and Ti_{A3}^0 centers are marked in Figs. 4 and 6 with dotted and solid lines, respectively.

The Ti^0 centers represent one of the cases for which no simple analytical expressions relating the transition fields with the spin-Hamiltonian parameters can be derived. The difficulties arise from the comparable order of magnitude of the hf and electronic Zeeman terms, the high anisotropy of the centers and the low local symmetry, reflected in the different orientations of the \hat{g} and \hat{A} tensors.¹⁸ Moreover, both principal values and principal directions of the spin-Hamiltonian tensors vary with the temperature. We thus have to resort to several approximations in order to obtain a qualitative description of the temperature dependence of the Ti^0 spectra.

In a simplified case, considering the \hat{g} and \hat{A} tensors to share the same orientation, the transition fields could be derived for the magnetic field parallel to one of the main directions. For \mathbf{B} parallel to z the expressions for the two transition fields are

$$B_{1,2} = \frac{(2h\nu \pm A_z)}{2g_z\mu_B} \sqrt{1 - \left(\frac{A_x}{2h\nu \pm A_z}\right)^2} \cdot \sqrt{1 - \left(\frac{A_y}{2h\nu \pm A_z}\right)^2}. \quad (9)$$

Similar expressions can be obtained along x and y , by cyclic permutations of g_i and A_i , where $i = x, y, z$.

From Eq. (9) one can notice that when the hf parameters are small enough compared to the microwave quantum $h\nu$, the difference $\Delta B_{res} = B_2 - B_1$ of the transition fields is proportional, in a good approximation, to the hf parameter along that specific direction of the magnetic field. This is expected to be valid for any random direction of the magnetic field. Therefore, the temperature dependence of the ΔB_{res} difference is expected to reflect mainly the variation of the sensitive hf parameters.

Figure 8 displays the temperature dependence of ΔB_{res} along the a crystal axis, in a temperature range covering both $C1c1$ and $P2_1cn$ phases, up to 170 K. At higher temperatures, up to the incommensurate phase, the transitions belonging to the two Ti_{A1}^0 and Ti_{A3}^0 centers could not be distinguished any longer. As in the case of the Ti^{2+} centers, an anomalous temperature dependence can be observed around the 74 K transition temperature, assigned to the coupling with the soft lattice modes. Above the transition temperature the variation is again almost linear for both centers.

The estimated errors for the transition fields range from ± 0.15 mT, where the individual lines are separated, to ± 0.5 mT where the lines overlap. The last case occurs around the transition point and at high temperatures ($T > 130$ K). To these errors an accuracy of ± 1 K in the temperature determination has to be added as well. Thus, some of the largest errors appear in a 30° temperature range cen-

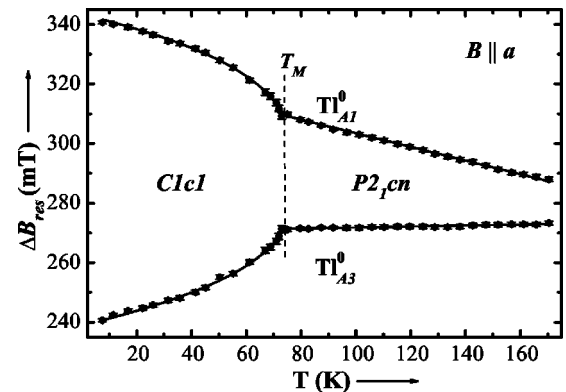


FIG. 8. Experimental temperature dependence of the difference of the resonance fields, ΔB_{res} , of the Ti_{A1}^0 and Ti_{A3}^0 type centers (solid circles) along the a direction in ferroelectric $\text{Rb}_2\text{ZnCl}_4:\text{Ti}$. Solid lines—the result of the fitting.

tered on the transition temperature, preventing an accurate analysis of the critical region. The temperature dependence of ΔB_{res} in the $C1c1$ phase was fitted with expression (6), where $T_c = T_M = 74$ K and $\gamma = 1$, using the same procedure as in the case of the Tl^{2+} centers, while the approximately linear behavior in the $P2_1cn$ phase was fitted with expression (7). The resulting fitting parameters are given in Table III and the calculated temperature dependencies are represented with solid lines in Fig. 8.

One can notice from Table III that the material constant C has the same value, within the experimental errors, for the two Tl^0 centers and a different one for the Tl^{2+} centers. This discrepancy may have multiple origins: in both cases we have considered the contribution of a single, dominant soft mode, neglecting the influence of the other lattice modes or of possible local modes, as observed in alkali halides.³⁰ The Tl^0 and Tl^{2+} centers are also expected to couple differently with the two soft modes of different symmetry. Moreover, the soft mode frequency was described with the simple expression (5), neglecting the influence of the macroscopic electric field, which is expected to differ for the Tl^0 and Tl^{2+} centers. It is also possible that the different coupling with the lattice for the Tl_{Ai}^0 and Tl^{2+} centers is related to a different localization of the impurity ion, which would then be at the Rb(2) and Rb(1) positions, respectively.

It is worth mentioning that, using the same theoretical model to describe the temperature induced g -value variation in the $C1c1$ phase of the Cu^{2+} (II) centers localized at Rb⁺ sites in Rb_2ZnCl_4 crystals,⁸ we found out a comparable value of $C = 9.7$ K^{1/2}.

The present paper shows how the study of the hyperfine splitting vs temperature dependence of the $6p^1$ - Tl^0 and $6s^1$ - Tl^{2+} centers yields valuable information concerning the SPT and associated lattice dynamics in the host lattice. This was possible because, despite the small relative variation of the hyperfine coupling with temperature, its large absolute value in the case of both Tl^0 and Tl^{2+} centers results in an enough large variation to be easily measured in the studied temperature range. In the case of the Mn^{2+} ions, which have been previously used to study the high temperature $P2_1cn \leftrightarrow INC$ and $INC \leftrightarrow Pmcn$ phase transitions^{6,7} in Rb_2ZnCl_4 crystals, the small value of the hyperfine coupling parameter ($A \approx 9$ mT), resulting from a different mechanism (core polarization³¹), is expected to yield, in the temperature range below 290 K, relative variations too small to be practically detectable. Indeed, determinations of the temperature induced variation of the hyperfine coupling parameter of Mn^{2+} ions in oxidic lattice hosts, such as $CaCO_3$ (calcite) (Ref. 32) and ThO_2 ,³³ resulted in total variations of less than 1% of A for the temperature range below 300 K and less than 0.1% of A for the temperature range below 100 K. In these cases, the corresponding temperature variation could be determined as a result of the very high accuracy in measuring the EPR lines position. This accuracy is determined by the

very small linewidth in these materials (smaller than $10 \mu T$ in the low temperature range). Because in crystals such as Rb_2ZnCl_4 the linewidth of the Mn^{2+} ions is orders of magnitude larger, the small temperature induced variations in the hyperfine coupling parameter associated with the local crystal field changes cannot be easily monitored. In the case of such paramagnetic transition ions, with $S > 1/2$, one prefers to study the temperature induced SPT with EPR by monitoring the more sensitive ZFS parameters from the spin Hamiltonian.¹¹

V. CONCLUSIONS

Thallium paramagnetic centers of $6p^1$ - Tl^0 and $6s^1$ - Tl^{2+} type were observed in the ferroelectric low temperature phases of x-ray irradiated $Rb_2ZnCl_4:Tl$ single crystals. Both centers are very likely localized at the two inequivalent Rb⁺ sites. Their visibility range allowed us to probe by EPR the $P2_1cn$ and $C1c1$ low temperature ferroelectric phases.

In the case of the s -type Tl^{2+} centers, the different values and orientations of the spin-Hamiltonian parameters determined at the three temperatures (90 K, 40 K and 26 K) reflect the changes in the local crystalline environment induced by the 74 K phase transition and the lattice dynamics in the $C1c1$ phase, as well.

Due to the mainly p -character of their electronic wave function and their relatively large hf parameter, the Tl^0 centers prove to be even more sensitive probes to the local crystal field changes induced by the SPTs and/or associated to the lattice dynamics. The temperature variation of their EPR spectra provides direct evidence of the unit cell tripling in the $P2_1cn$ phase, the symmetry lowering in the $C1c1$ phase and the lattice dynamics in both low temperature ferroelectric phases. The different symmetry of these two phases is reflected in the larger number of inequivalent centers present in the lowest temperature $C1c1$ phase and in the different values and orientation of the Tl^0 centers spin-Hamiltonian parameters in the two phases.

The temperature variation of the spectra belonging to both types of centers is explained by the influence of the soft modes in the monoclinic $C1c1$ phase, while in the commensurate orthorhombic $P2_1cn$ phase the interplay between the thermal expansion of the lattice and the influence of the other excited lattice modes leads to the observed linear variation with temperature.

ACKNOWLEDGMENTS

The present work was performed in the frame of the bilateral scientific project BIL 00/72 between Flanders (Belgium) and Romania and of the Ceres scientific Project No. 31/2001 of the Ministry of Education and Research of Romania. Further financial support by the Fund for Scientific Research–Flanders is kindly acknowledged.

- *Electronic address: mstefan@alpha1.infim.ro
- ¹H.Z. Cummins, Phys. Rep. **185**, 211 (1990).
- ²M. Quilichini and J. Pannetier, Acta Crystallogr., Sect. B: Struct. Sci. **39**, 657 (1983).
- ³F.J. Lopez and A. Martin, Phys. Rev. B **38**, 6392 (1988).
- ⁴S.V. Nistor, A. Bouwen, and D. Schoemaker, Phys. Status Solidi B **189**, 345 (1995).
- ⁵M. Stefan, S.V. Nistor, N.M. Grecu, and D. Schoemaker, Phys. Status Solidi B **202**, 999 (1997).
- ⁶J.J.L. Horikx, A.F.M. Arts, and H.W. de Wijn, Phys. Rev. B **37**, 7209 (1988), and references cited therein.
- ⁷A. Kassiba, M. Pezeril, P. Molinie, and J. Fayet, Phys. Rev. B **40**, 54 (1989), and references cited therein.
- ⁸M. Stefan, S.V. Nistor, D. Schoemaker, and I. Ursu, Solid State Commun. **127**, 695 (2003).
- ⁹S.V. Nistor, Mater. Sci. Forum **239-241**, 543 (1997), and references cited therein.
- ¹⁰M. Stefan, S.V. Nistor, D.C. Mateescu, and A.M. Abakumov, J. Cryst. Growth **200**, 148 (1999).
- ¹¹K.A. Muller and J.C. Fayet, *Structural Phase Transitions II*, Topics in Current Physics, Vol. 23 (Springer-Verlag, Berlin, 1991), p. 1.
- ¹²A. Ranfagni, D. Mugnai, and M. Bacci, Adv. Phys. **32**, 823 (1983), and references cited therein.
- ¹³M. Stefan, S.V. Nistor, and D. Schoemaker, Radiat. Eff. Defects Solids **150**, 365 (1999).
- ¹⁴M. Stefan, S.V. Nistor, and D. Schoemaker, Radiat. Eff. Defects Solids **155**, 373 (2001).
- ¹⁵S.V. Nistor, D. Schoemaker, and I. Ursu, Phys. Status Solidi B **185**, 9 (1994), and references cited therein.
- ¹⁶C.J. Delbecq, W. Hayes, M.C.M. O'Brian, and P.H. Yuster, Proc. R. Soc. London, Ser. A **271**, 243 (1963).
- ¹⁷S.V. Nistor, I. Heynderickx, E. Goovaerts, A. Bouwen, and D. Schoemaker, Phys. Status Solidi B **130**, 175 (1985).
- ¹⁸E. Goovaerts, J. Andriessen, S.V. Nistor, and D. Schoemaker, Phys. Rev. B **24**, 29 (1981).
- ¹⁹A. Abragam and B. Bleaney, *Electron Paramagnetic Resonance of Transition Ions* (Clarendon Press, Oxford, 1970).
- ²⁰*Computer Program EPR-NMR*, Dept. of Chemistry, Univ. of Saskatchewan, Canada (1993).
- ²¹D. Schoemaker, Phys. Rev. B **7**, 786 (1973).
- ²²D. Schoemaker, I. Heynderickx, and E. Goovaerts, Phys. Rev. B **31**, 5687 (1985).
- ²³K. Itoh, A. Hinasada, H. Matsunaga, and E. Nakamura, J. Phys. Soc. Jpn. **52**, 664 (1983).
- ²⁴M. Wada, A. Sawada, and Y. Ishibashi, J. Phys. Soc. Jpn. **50**, 531 (1981), and references cited therein.
- ²⁵M. Quilichini, V. Dvorak, and P. Boutrouille, J. Phys. I **1**, 1321 (1991).
- ²⁶K. Tsuchida and R. Abe, J. Phys. Soc. Jpn. **46**, 1225 (1979).
- ²⁷M.N. Grecu, D.P. Lazar, and V.V. Grecu, in *Proceedings of the XII International Conference on Defects in Insulating Materials, Schloss Nordkirchen, Germany, 1992*, edited by O. Kanert and J.M. Spaeth (World Scientific, Singapore, 1993), Vol. 1, p. 633.
- ²⁸R. Blinc and B. Zeks, *Soft Modes in Ferroelectrics and Antiferroelectrics* (North-Holland, Amsterdam, 1974).
- ²⁹W.M. Walsh, Jr., J. Jeener, and N. Bloembergen, Phys. Rev. **139**, A1338 (1965).
- ³⁰W. Joosen, E. Goovaerts, and D. Schoemaker, Phys. Rev. B **32**, 6748 (1985).
- ³¹R.E. Watson and A.J. Freeman, *Hyperfine Interactions* (Academic Press, New York, 1967).
- ³²R.A. Serway, Phys. Rev. B **3**, 608 (1971).
- ³³S.A. Marshall, S.V. Nistor, C.-Y. Huang, and T. Marshall, Phys. Status Solidi B **59**, 55 (1973).